## Superballistic Paradox in Electron Fluids: Relevance of Tomographic Transport

Jorge Estrada-Álvarez, Elena Díaz<sup>®</sup>, and Francisco Domínguez-Adame<sup>®</sup> GISC, Departamento de Física de Materiales, Universidad Complutense, E-28040 Madrid, Spain

(Received 25 February 2025; revised 30 June 2025; accepted 9 October 2025; published 12 November 2025)

Electron hydrodynamics encompasses the exotic fluidlike behavior of electrons in two-dimensional materials such as graphene. It accounts for superballistic conduction, also known as the Gurzhi effect, where increasing temperature reduces the electrical resistance. In analogy with conventional fluids, the Gurzhi effect is only expected in the hydrodynamic regime, with the decrease in the resistance occurring at intermediate temperatures. Nonetheless, experiments on electron fluids consistently show that superballistic conduction starts at close-to-zero temperature. To address this paradox, we study hydrodynamic flow, and we find that replacing the conventional dynamics with tomographic dynamics gives rise to an accurate low-temperature description. The latter strengthens superballistic conduction, with potential applications in low-dissipation devices, and explains its differences with the Molenkamp effect and conventional fluid dynamics. Our study reveals that the superballistic paradox is resolved by considering the peculiarities of electron-electron collisions at the Fermi surface.

DOI: 10.1103/xsjh-lq5h

The pursuit of miniaturization of electronic devices faces the inherent challenge of energy dissipation [1], and further optimizing the devices relies on our ability to mitigate the increased electrical resistance. A feasible strategy to achieve this goal is to use the Gurzhi effect, exploiting electrons' hydrodynamic behavior [2–4]. Electron hydrodynamics substitutes ohmic transport in many twodimensional (2D) materials, such as graphene and gallium arsenide heterostructures [5–10], or PdCoO<sub>2</sub> [11]. Electron fluids exhibit exotic signatures [12,13], from Poiseuille's flow [14,15] to the formation of whirlpools [16–19]. These features have potential applications in 2D devices, including high-frequency operation [20,21] and the Gurzhi effect [22,23]. This effect exploits the collective motion of electrons to evade scattering against the device's edges. Therefore, the resistance is lower than the ballistic limit, resulting in superballistic conduction and enabling devices with reduced dissipation [24-28].

The Gurzhi effect involves a decreasing electrical resistance at intermediate temperatures, as depicted schematically in Fig. 1(a). The flow is mostly ballistic at low temperatures, but increasing temperature favors electron-electron collisions and leads to viscous electron flow. Thus, the Gurzhi effect would only occur at intermediate temperatures [22], once the distance that electrons travel before colliding with other electrons is shorter than the size of the

Published by the American Physical Society under the terms of the Creative Commons Attribution 4.0 International license. Further distribution of this work must maintain attribution to the author(s) and the published article's title, journal citation, and DOI. device, namely,  $l_{ee} < d$ . More precisely, as Gurzhi later suggested for 2D systems [29], when  $l_{ee} \sqrt{T/T_F} < d$ , where  $T_F$  is the Fermi temperature. Since  $l_{ee} \sim 1/T^2$  [3], both conditions imply that the Gurzhi effect is expected to occur above a finite threshold temperature. Except for collisions with phonons, which raise the resistance at even higher temperatures, most of the Gurzhi effect would resemble the behavior of a conventional fluid: at low collision rates, the resistance increases with collisions until it reaches a maximum or, equivalently, a minimum current, known as the Knudsen minimum in conventional fluids [30,31].

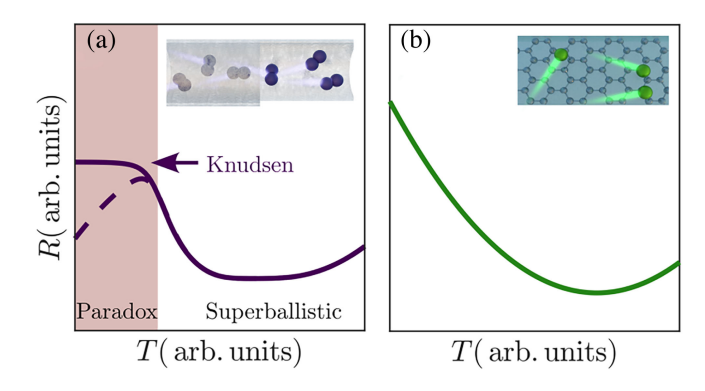


FIG. 1. Superballistic paradox scheme. (a) Inspired by conventional fluids, Gurzhi suggested a decrease in the electrical resistance of metals with increasing temperatures. The latter would only occur above a finite threshold temperature, where the Knudsen minimum of the current (i.e., maximum of the resistance) arises [22]. (b) On the contrary, experiments with electron fluids show that the decrease starts at close-to-zero temperature [7,8,26,32–35].

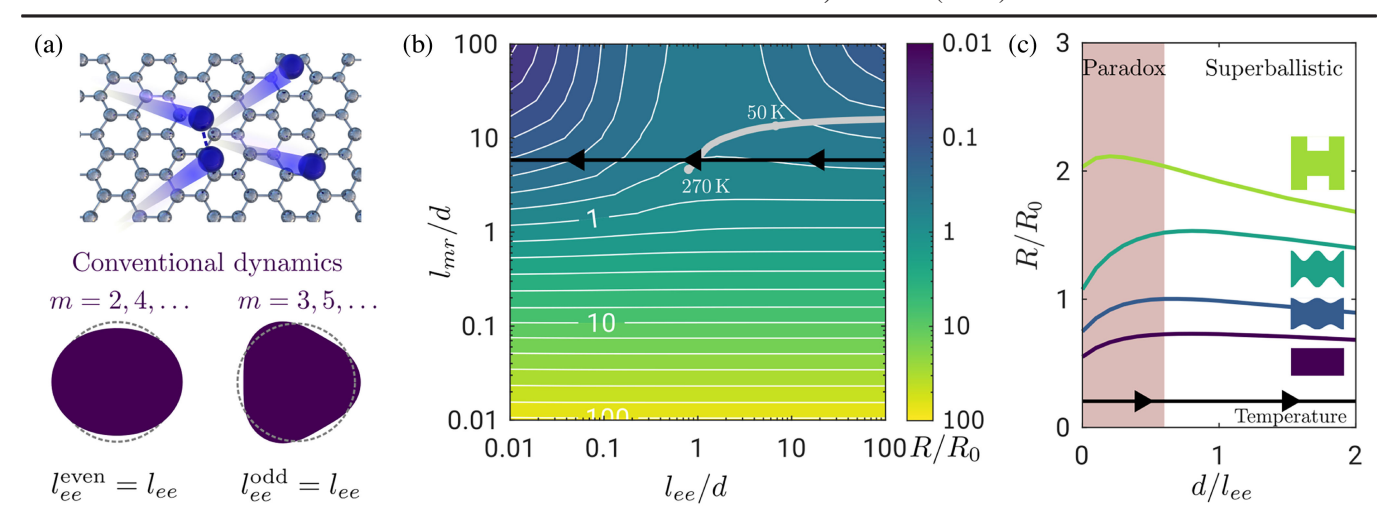


FIG. 2. Conventional dynamics. (a) Electrons can collide regardless of their direction of movement, allowing for the relaxation of the even and odd parity modes. (b) Resistance of a uniform channel as a function of the collision rates,  $l_{ee}$  and  $l_{mr}$ . The gray line shows typical values for a graphene channel of width d=200 nm at  $n=0.5\times10^{12}$  cm<sup>-2</sup> [18,26]. (c) Resistance as a function of  $l_{ee}^{-1}\sim T^2$ . At low temperatures, the resistance first increases with temperature, but after a threshold, it decreases. Therefore, conventional dynamics predict a significant increase in the resistance for  $l_{ee}\gtrsim d$ , not observed in the experiments. We show the results for a constriction and uniform and crenellated channels with increasing corrugation at  $l_{mr}/d=5$ .

Progress in 2D materials has enabled the realization of the superballistic effect predicted by Gurzhi. However, experiments performed in graphene and gallium arsenide heterostructures show a different behavior: The decrease in the resistance starts at close-to-zero temperatures [7,8,26,32–35], as shown schematically in Fig. 1(b), and no signatures of the Knudsen minimum of the current are observed. Thus, experimental evidence supports the prediction of resistance reduction due to electron-electron collisions [36]. Still, such reduction is already effective at temperatures much lower than estimated by Gurzhi.

In this Letter, we investigate this *superballistic paradox* and sort it out by considering the electron microscopic dynamics. The unexpected superballistic conduction observed at low temperatures affects the fundamentals of the Gurzhi effect, and it supports the tomographic description [37], which we analyze in the limit of close-to-zero temperature.

Let us consider the polar distribution function  $g(\mathbf{r}, \theta)$  that accounts for the excess of electrons above the Fermi distribution at position  $\mathbf{r}$  moving in the direction of  $\theta$ . It satisfies the following steady state Boltzmann transport equation [36,38–44]:

$$\begin{pmatrix} \cos \theta \\ \sin \theta \end{pmatrix} \cdot \nabla_{\mathbf{r}} \left( g - \frac{\mathrm{eV}}{\hbar k_F} \right) = -\frac{g}{l_{mr}} + \Gamma_{ee}[g], \qquad (1)$$

where  $k_F$  is the Fermi wave number, V(r) is the electric potential, and, according to experiments, a constant carrier density n is set [8,26,34]. This description, although approximate at temperatures that are a fraction of the Fermi temperature, is reliable in the low temperature limit where we aim to characterize the initial increase or decrease of the resistance. The Fermi liquid approach is also

consistent with experimental evidence [26], obtained at intermediate carrier densities where the superballistic effect can be distinguished from a thermal activation mechanism [45]. It is worth mentioning that the Boltzmann transport equation not only enables the description of the hydrodynamic regime but also the ballistic one. Staying away from charge neutrality also avoids energy-dependent scattering, as in the explanation proposed for the Wiedemann-Franz law's violation [46]. Therefore, we consider a momentum-relaxing scattering against defects and phonons through the mean free path  $l_{mr}$ , as well as electron-electron collisions via the collision operator  $\Gamma_{ee}$  [47–50]. Once we solve Eq. (1) by the finite element method with the proper boundary conditions [41,44,51,52], we can compute the drift velocity as  $u(r) = (1/\pi) \int_0^{2\pi} g(r, \theta) (\cos \theta, \sin \theta) d\theta$  to get the electric current and the resistance R of a device. We simulate constrictions of width d, where  $R_0 = \hbar k_F/ne^2 d$ , and crenellated channels of average width d, where  $R_0 =$  $\hbar k_F L/ne^2 d^2$  and  $L \gg d$  is the length of the channel, long enough to ignore the contacts.

In analogy with ordinary fluids, let us first consider electron conventional dynamics, where two electrons can collide regardless of their momentum orientation, as depicted in Fig. 2(a). Hence, the collision operator reads

$$\Gamma_{ee}[g] = -\frac{g - g_{ee}}{l_{ee}},\tag{2}$$

where  $l_{ee}$  is the electron-electron mean free path and  $g_{ee} = u_x \cos \theta + u_y \sin \theta$  is a polar distribution with the average velocity of the electrons [41]. It is important to remark that Eq. (2), which accounts for Callaway's ansatz [53],

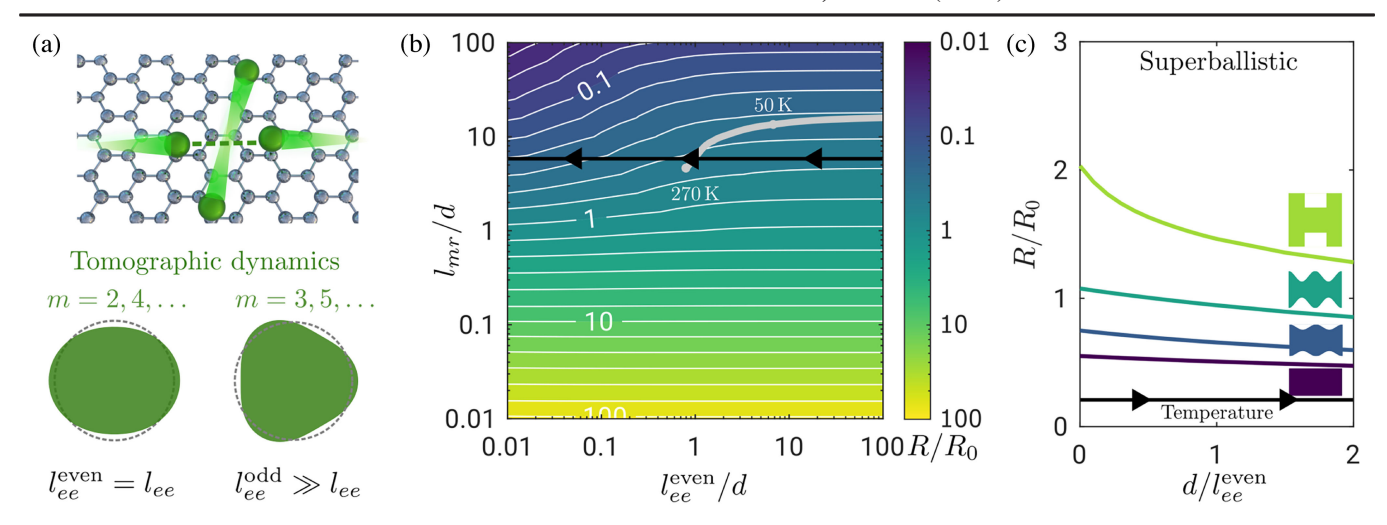


FIG. 3. Tomographic dynamics. (a) Only head-on collisions are allowed between electrons, so odd parity modes do not relax. (b) Resistance as a function of the collision rates in the limit of close-to-zero temperature  $l_{ee}^{\text{even}}/l_{ee}^{\text{odd}}=0$  [44]. The gray line shows typical values for a graphene channel of width d = 200 nm at  $n=0.5\times10^{12}$  cm<sup>-2</sup> [18,26]. (c) The resistance decreases with electron-electron collisions in a constriction and uniform and crenellated channels, for  $l_{mr}/d=5$ , even for close-to-zero temperature in agreement with the experiments.

assumes the relaxation of all modes with  $m \ge 2$  in the expansion  $g = \sum_{m} (c_m \cos m\theta + s_m \sin m\theta)$ .

Figure 2(b) shows the simulated resistance of a channel of width d. Notice that experiments typically study superballistic conduction when  $l_{\rm mr} > d$ , reaching up to  $l_{\rm mr}/d \gtrsim 10$  [26,44]. Moreover, the resistance drop also enhances for the smallest devices, so the region with  $l_{\rm mr} \lesssim d$  cannot be used to solve the superballistic paradox. For  $l_{\rm mr} \gtrsim d$ , it is not until  $l_{ee} \lesssim d$  when transport is collective and parallel electrons no longer dominate, that the Gurzhi effect would occur. In such a fluid regime, collisions between electrons keep them from colliding with the edges. Although in the absence of electron-electron collisions, electrons travel a distance d, in their presence, they move in shorter steps of length  $l_{ee}$ . Thus, on average, they propagate a distance  $d^2/l_{ee}$  before reaching the edge, reducing the resistance [22].

Figure 2(c) shows the resistance for a constriction, uniform, and crenellated channels, where the bending of the electron trajectories triggers the dependence of the resistance on electron collisions [8]. While the curves reproduce the behavior for ordinary fluids, experiments on electrons show no initial increase nor plateau, giving rise to the superballistic paradox. This rise is conspicuous when the device has well-defined transport directions, since electron-electron collisions deviate the electrons from them, contributing to the resistance. In addition, we can also prove that the initial resistance increase would arise, or even worsen, for other edge scattering mechanisms [54,55] and  $l_{mr}/d$  ratios [44]. As we will discuss, the superballistic paradox originates in the properties of electron-electron collisions

We now discuss the experimental evidence demonstrating that a lack of measurements at low enough temperature cannot

be responsible for the observed paradox [44]. For a typical size  $d \sim 0.2 \,\mu\text{m}$  and a density of carriers  $n = 0.5 \times 10^{12} \,\text{cm}^{-2}$ , the temperature at which the original Gruzhi condition for superballistic conduction fulfills ( $l_{ee} < d$ ) is 200 K in graphene devices [26,34]. Similarly in gallium arsenide heterostructures at  $n = 0.25 \times 10^{12} \text{ cm}^{-2}$ , it is not until 10 K that we reach  $l_{lee} \sim 1 \, \mu \text{m}$ , the characteristic size of the device [8]. However, in both 2D electron systems, experiments have observed a decrease in the resistance due to the superballistic effect for temperature far below the Gurzhi threshold estimated above. Additionally, no increase in resistance was observed at close-to-zero temperature, where measurements were performed. This behavior has been confirmed in several experimental setups [7,8,26,32–35]. Hence, the observed paradox is not exclusive to a particular material or geometry that prompts us to seek a proper explanation.

Now, let us get a deeper insight into the differences between conventional and electron fluids to settle the superballistic paradox. Indeed, unlike molecules in classical fluids that follow a Maxwell distribution, electrons are fermions governed by the Fermi-Dirac statistics. The conservation of energy and momentum in a 2D system and the need for occupied initial and unoccupied final states in scattering events highly restrict collisions. At low temperature, these are predominantly head-on collisions among electrons facing each other, resulting in the tomographic dynamics [29,37,56–63] depicted in Fig. 3(a). To restrict our model to tomographic dynamics, we need to split the collision operator as follows

$$\Gamma_{ee}[g] = -\sum_{m} \frac{g^{(m)} - g^{(m)}_{ee}}{I^{(m)}_{ee}},$$
(3)

where  $l_{ee}^{(m)}$  is the decay length corresponding to the  $m{\rm th}$ mode of the expansion of g. The even modes have a characteristic length  $l_{ee}^{\text{even}}$ . However, at low temperature, the odd-parity modes m=3,5... have a decay length such as  $l_{ee}^{(m)} \sim m^4 (T_F/T)^2 l_{ee}^{\rm even}$  [44,64]. Therefore, in the low-temperature limit,  $l_{ee}^{\rm odd} \gg l_{ee}^{\rm even}$ . As a first approach to distinguish whether the resistance increases or decreases at close-to-zero temperature, we will consider  $l_{ee}^{\text{even}}/l_{ee}^{\text{odd}} =$ 0 as a limiting situation of tomographic dynamics. This approach allows us to circumvent an explicit treatment of the functional dependence of the decay lengths on the ratio  $T/T_F$ . At intermediate temperatures the electrical response would result from the combination of conventional dynamics and the limiting situation where the odd modes do not relax. Therefore, a separate evaluation of each mode would be required to describe the full temperature range of experiments [26,44,65,66]. Under tomographic dynamics, head-on collisions do not relax the odd modes, and it is not trivial to determine their impact on the macroscopic properties. Hydrodynamic models akin to the Navier-Stokes equation are blind to the distinction between even and odd parity modes [41,44], and thus, enable us to account for the tomographic dynamics. However, the Boltzmann equation distinguishes them, resulting in a crucial theoretical tool to explain the paradox.

The resistance map in Fig. 3(b) shows key differences from its conventional counterpart of Fig. 2(b), and Fig. 3(c) shows the resistance curves. The Landauer-Sharvin limit for a constriction  $R = 1.57R_0$ , together with the Ohmic contribution of the whole device, gives the total simulated resistance of Fig. 3(c) [26]. The consideration of the full collision operator (3), with different relaxation rates for the odd modes, is needed to reproduce quantitative results. Still,  $l_{ee}^{\text{even}}/l_{ee}^{\text{odd}} = 0$  qualitatively captures the decrease in the resistance at close-to-zero temperature [44]. Tomographic dynamics predict no increase in the resistance but a decrease starting at close-to-zero temperature, consistent with the experiments, thus solving the paradox. Since the electric current is mainly associated with the odd-parity modes, it is no wonder that tomographic dynamics do not exhibit the initial increase in the resistance characteristic of conventional dynamics. Indeed, head-on collisions cannot bring the electrons out of their trajectories parallel to the channel [43] and increase the resistance.

Theoretical studies predict how tomographic dynamics correct current injectors [67], thermoelectric properties [68], or the Poiseuille flow [37]. However, experiments have explained Poiseuille's flow without noticing the subtle difference yet [14]. The search for experimental evidence of tomographic dynamics includes the analysis of magnetotransport in ultrapure devices [39,69] and of the scaling d ln R/d ln T [64]. The latter changes with the transport regime [66] and depends on a previous assumption of the mean free path temperature scaling,  $l_{ee} \sim T^{-2}$  [3] or

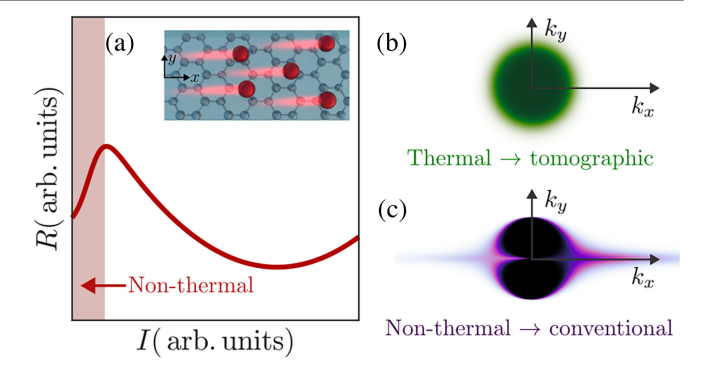


FIG. 4. Molenkamp effect scheme. (a) Resistance as a function of the current. (b) The Fermi electron distribution. (c) The nonthermal electron distribution has many electrons traveling parallel to the channel. The collisions are now closer to conventional dynamics, resulting in an increasing resistance.

 $l_{ee} \sim T^{-2} \ln(T_F/T)$  [26], as well as for the odd parity modes [26]. Our proposal to solve the superballistic paradox results in clear experimental evidence of the tomographic dynamics that only assumes that temperature favors collisions between electrons, a direct consequence of the Pauli blockade [3]. Furthermore, our approach is not based on a change in the peculiarities of the scaling behavior of R(T). In contrast to previous studies [64], under a proper description of edge scattering beyond the nonphysical noslip boundary condition [44,55,70,71], we demonstrate that conventional dynamics lead to an initial increase in the resistance, in agreement with standard fluids [30,31].

We have already demonstrated that conventional and tomographic dynamics yield a Gurzhi effect in 2D electronic systems. However, in the first case, the superballistic effect arises at intermediate temperature. In contrast, in the second scenario, it already starts at close-to-zero temperature. Since electron dynamics is tomographic at low temperature, we have confirmed that the reduction of the resistance starts at zero temperature, in agreement with experiments [7,8,26,32–35]. However, a different behavior was found in Molenkamp's experiment [21,72-74], where, instead of increasing temperature, high electric currents were used. In such a case, the rate of electron-electron collisions rises due to the applied current. We schematically show Molenkamp's experimental results in channels in Fig. 4(a). Remarkably, and contrary to the measurements obtained for increasing temperature, Molenkamp's work reported an initial increase in the resistance at low currents. namely, at low electron-electron collision rates. After this experiment, Gurzhi adapted their original predictions for the superballistic effect in a metal  $(l_{ee} < d)$ , for a 2D tomographic electron system to demonstrate a decrease in the resistance for an easier condition to fulfill, namely,  $l_{ee}\sqrt{T/T_F} < d$  [29]. The latter would lead to a decrease in the resistance for lower temperature consistently with Molenkamp's experiment. Once again, for graphene at n = $0.5 \times 10^{12} \ {\rm cm^{-2}}$  the new condition  $l_{ee} \sqrt{T/T_F} \sim d \sim$ 0.2 µm would be valid above 70 K [18,26]. However experiments do not reveal any data compatible with a Knudsen minimum in the electric current at such temperature neither. Remarkably, our simulations under the tomographic approach demonstrate that the resistance decreases regardless of the condition  $l_{ee}\sqrt{T/T_F} < d$ , which was not possible to spot by analytic calculations [29].

The peculiarity of the Molenkamp effect, with a starting increase in the resistance, lies in the lack of thermal equilibrium. When the device's temperature rises, electrons still follow the Fermi distribution. However, if a high current is applied, it mainly accelerates those electrons traveling parallel to the channel, and their distribution is no longer thermal. Tomographic dynamics is derived under the assumption of 2D electrons within the Fermi distribution, as shown in Fig. 4(b). Thus, it is no wonder its failure to describe Molenkamp's results where the distribution is nonthermal, like the one depicted in Fig. 4(c). Notice that an arbitrary electron will mostly collide with another electron moving parallel to the channel since the distribution is much broader in that direction [44]. Indeed, these new collisions overshadow the head-on tomographic ones for sharper distribution functions. To support our analysis we solve the collision integrals [59,62] for the non-thermal distribution and demonstrate that  $l_{ee}^{\text{even}}$  and  $l_{ee}^{\text{odd}}$  are comparable in that case, so that tomographic dynamics  $(l_{ee}^{\text{odd}} \gg l_{ee}^{\text{even}})$  no longer applies [44]. Instead, the obtained behavior is close to the one described by conventional dynamics that gives rise to an initial resistance increase, as previously demonstrated.

The application of even higher currents and the activation of more electronic collisions eventually lead to the thermalization of the Fermi distribution. The latter and the increase in  $d/l_{ee}^{\rm even}$  contribute to the decreasing resistance observed in Molenkamp's experiment. The Molenkamp effect, which seemed to be an exception in our theory, reinforces our analysis. Physical scenarios without thermal equilibrium opened a window for conventional dynamics.

In conclusion, we demonstrate that even details of electron dynamics dramatically alter their electrical properties. At low temperature, conventional dynamics lead to an increase in resistance upon rising temperature, while tomographic dynamics, in the limit where the odd modes do not relax, lead to a decrease in resistance. Experiments show a decrease in the resistance even at close-to-zero temperature, with no signature supporting the so-called Knudsen minimum of electric current, which is consistent with our tomographic simulations. Therefore, this electron's anomaly signals the occurrence of tomographic dynamics, strengthening the superballistic effect and enabling its application to low-dissipation devices. Our theory explains the different behavior between electrons and conventional fluids and, by considering current-driven nonthermal phenomena, it provides a plausible explanation of the Molenkamp effect. We ultimately solve the superballistic paradox, which is a consequence of the peculiarities of electron-electron collisions at the Fermi surface.

Acknowledgments—We thank R. Brito, J. Salvador-Sánchez, M. Amado, and E. Diez for discussions. This work was supported by the "(MAD2D-CM)-UCM" project funded by Comunidad de Madrid, by the Recovery, Transformation, and Resilience Plan, and by NextGenerationEU from the European Union and Agencia Estatal de Investigación of Spain (Grant No. PID2022-136285NB-C31). J. E.-A. acknowledges support from the Spanish Ministerio de Ciencia, Innovación y Universidades (Grant No. FPU22/01039).

Data availability—The data are not publicly available. The data are available from the authors upon reasonable request.

- [1] G. Varnavides, A. Yacoby, C. Felser, and P. Narang, Charge transport and hydrodynamics in materials, Nat. Rev. Mater. **8**, 726 (2023).
- [2] B. N. Narozhny, Hydrodynamic approach to two-dimensional electron systems, Riv. Nuovo Cimento 45, 661 (2022).
- [3] M. Polini and A. K. Geim, Viscous electron fluids, Phys. Today 73, No. 6, 28 (2020).
- [4] G. Baker, M. Moravec, and A. P. Mackenzie, A perspective on non-local electronic transport in metals: Viscous, ballistic, and beyond, Ann. Phys. (Amsterdam) 536, 2400087 (2024).
- [5] Y. A. Pusep, M. D Teodoro, V. Laurindo Jr, E. R. Cardozo de Oliveira, G. Gusev, and A. K. Bakarov, Diffusion of photoexcited holes in a viscous electron fluid, Phys. Rev. Lett. 128, 136801 (2022).
- [6] P. S. Alekseev, Negative magnetoresistance in viscous flow of two-dimensional electrons, Phys. Rev. Lett. 117, 166601 (2016).
- [7] D. I. Sarypov, D. A. Pokhabov, A. G. Pogosov, E. Y. Zhdanov, A. A. Shevyrin, A. K. Bakarov, and A. A. Shklyaev, Temperature dependence of electron viscosity in superballistic GaAs point contacts, Phys. Rev. Lett. 134, 026302 (2025).
- [8] A. C. Keser, D. Q. Wang, O. Klochan, D. Y. H. Ho, O. A. Tkachenko, V. A. Tkachenko, D. Culcer, S. Adam, I. Farrer, D. A. Ritchie, O. P. Sushkov, and A. R. Hamilton, Geometric control of universal hydrodynamic flow in a two-dimensional electron fluid, Phys. Rev. X 11, 031030 (2021).
- [9] Z. T. Wang, M. Hilke, N. Fong, D. G. Austing, S. A. Studenikin, K. W. West, and L. N. Pfeiffer, Nonlinear transport phenomena and current-induced hydrodynamics in ultrahigh mobility two-dimensional electron gas, Phys. Rev. B 107, 195406 (2023).
- [10] A. Gupta, J. J. Heremans, G. Kataria, M. Chandra, S. Fallahi, G. C. Gardner, and M. J. Manfra, Hydrodynamic and ballistic transport over large length scales in GaAs/AlGaAs, Phys. Rev. Lett. 126, 076803 (2021).
- [11] P. J. Moll, P. Kushwaha, N. Nandi, B. Schmidt, and A. P. Mackenzie, Evidence for hydrodynamic electron flow in PdCoO<sub>2</sub>, Science **351**, 1061 (2016).
- [12] A. Talanov, J. Waissman, A. Hui, B. Skinner, K. Watanabe, T. Taniguchi, and P. Kim, Observation of electronic viscous

- dissipation in graphene magneto-thermal transport, arXiv:2406.13799.
- [13] R. Sano and M. Matsuo, Breaking down the magnonic Wiedemann-Franz law in the hydrodynamic regime, Phys. Rev. Lett. **130**, 166201 (2023).
- [14] J. A. Sulpizio, L. Ella, A. Rozen, J. Birkbeck, D. J. Perello, D. Dutta, M. Ben-Shalom, T. Taniguchi, K. Watanabe, T. Holder *et al.*, Visualizing Poiseuille flow of hydrodynamic electrons, Nature (London) **576**, 75 (2019).
- [15] A. Jenkins, S. Baumann, H. Zhou, S. A. Meynell, Y. Daipeng, K. Watanabe, T. Taniguchi, A. Lucas, A. F. Young, and A. C. Bleszynski Jayich, Imaging the breakdown of ohmic transport in graphene, Phys. Rev. Lett. 129, 087701 (2022).
- [16] A. Aharon-Steinberg, T. Völkl, A. Kaplan, A. K. Pariari, I. Roy, T. Holder, Y. Wolf, A. Y. Meltzer, Y. Myasoedov, M. E. Huber *et al.*, Direct observation of vortices in an electron fluid, Nature (London) 607, 74 (2022).
- [17] M. L. Palm, C. Ding, W. S. Huxter, T. Taniguchi, K. Watanabe, and C. L. Degen, Observation of current whirlpools in graphene at room temperature, Science 384, 465 (2024).
- [18] D. Bandurin, I. Torre, R. K. Kumar, M. Ben Shalom, A. Tomadin, A. Principi, G. Auton, E. Khestanova, K. Novoselov, I. Grigorieva *et al.*, Negative local resistance caused by viscous electron backflow in graphene, Science 351, 1055 (2016).
- [19] G. Falkovich and L. Levitov, Linking spatial distributions of potential and current in viscous electronics, Phys. Rev. Lett. 119, 066601 (2017).
- [20] M. Kravtsov, A. L. Shilov, Y. Yang, T. Pryadilin, M. A. Kashchenko, O. Popova, M. Titova, D. Voropaev, Y. Wang, K. Shein *et al.*, Viscous terahertz photoconductivity of hydrodynamic electrons in graphene, Nat. Nanotechnol. 20, 51 (2024).
- [21] J. Estrada-Álvarez, E. Díaz, and F. Dominguez-Adame, Negative differential resistance of viscous electron flow in graphene, 2D Mater. 12, 015012 (2024).
- [22] R. N. Gurzhi, Minimum of resistance in impurity-free conductors, Sov. Phys. JETP **17**, 521 (1963), http://www.jetp.ras.ru/cgi-bin/e/index/e/17/2/p521?a=list.
- [23] R. N. Gurzhi, Hydrodynamic effects in solids at low temperature, Sov. Phys. Usp. 11, 255 (1968).
- [24] W. Huang, T. Paul, M. L. Perrin, and M. Calame, Eliminating the channel resistance in two-dimensional systems using viscous charge flow, 2D Mater. 11, 033001 (2024).
- [25] A. Stern, T. Scaffidi, O. Reuven, C. Kumar, J. Birkbeck, and S. Ilani, How electron hydrodynamics can eliminate the Landauer-Sharvin resistance, Phys. Rev. Lett. 129, 157701 (2022).
- [26] R. Krishna Kumar, D. Bandurin, F. Pellegrino, Y. Cao, A. Principi, H. Guo, G. Auton, M. Ben Shalom, L. A. Ponomarenko, G. Falkovich *et al.*, Superballistic flow of viscous electron fluid through graphene constrictions, Nat. Phys. 13, 1182 (2017).
- [27] H. Guo, E. Ilseven, G. Falkovich, and L. S. Levitov, Higher-than-ballistic conduction of viscous electron flows, Proc. Natl. Acad. Sci. U.S.A. 114, 3068 (2017).
- [28] J. Estrada-Álvarez, F. Bermúdez-Mendoza, F. Domínguez-Adame, and E. Díaz, Optimal geometries for low-resistance viscous electron flow, Phys. Rev. B 111, 075401 (2025).

- [29] R. N. Gurzhi, A. N. Kalinenko, and A. I. Kopeliovich, Electron-electron collisions and a new hydrodynamic effect in two-dimensional electron gas, Phys. Rev. Lett. 74, 3872 (1995).
- [30] M. Knudsen, Die Gesetze der Molekularströmung und der inneren Reibungsströmung der Gase durch Röhren, Ann. Phys. (Berlin) **333**, 75 (1909).
- [31] G. Tatsios, S. K. Stefanov, and D. Valougeorgis, Predicting the Knudsen paradox in long capillaries by decomposing the flow into ballistic and collision parts, Phys. Rev. E 91, 061001(R) (2015).
- [32] V. T. Renard, O. A. Tkachenko, V. A. Tkachenko, T. Ota, N. Kumada, J.-C. Portal, and Y. Hirayama, Boundary-mediated electron-electron interactions in quantum point contacts, Phys. Rev. Lett. **100**, 186801 (2008).
- [33] L. V. Ginzburg, C. Gold, M. P. Röösli, C. Reichl, M. Berl, W. Wegscheider, T. Ihn, and K. Ensslin, Superballistic electron flow through a point contact in a Ga[Al]As heterostructure, Phys. Rev. Res. 3, 023033 (2021).
- [34] J. Estrada-Álvarez, J. Salvador-Sánchez, A. Pérez-Rodríguez, C. Sánchez-Sánchez, V. Clericò, D. Vaquero, K. Watanabe, T. Taniguchi, E. Diez, F. Domínguez-Adame et al., Superballistic conduction in hydrodynamic antidot graphene superlattices, Phys. Rev. X 15, 011039 (2025).
- [35] L. V. Ginzburg, Y. Wu, M. P. Röösli, P. R. Gomez, R. Garreis, C. Tong, V. Stará, C. Gold, K. Nazaryan, S. Kryhin *et al.*, Long distance electron-electron scattering detected with point contacts, Phys. Rev. Res. 5, 043088 (2023).
- [36] K. E. Nagaev and O. S. Ayvazyan, Effects of electronelectron scattering in wide ballistic microcontacts, Phys. Rev. Lett. 101, 216807 (2008).
- [37] P. Ledwith, H. Guo, A. Shytov, and L. Levitov, Tomographic dynamics and scale-dependent viscosity in 2D electron systems, Phys. Rev. Lett. **123**, 116601 (2019).
- [38] A. N. Afanasiev, P. S. Alekseev, A. A. Greshnov, and M. A. Semina, Ballistic-hydrodynamic phase transition in flow of two-dimensional electrons, Phys. Rev. B 104, 195415 (2021).
- [39] H. Rostami, N. Ben-Shachar, S. Moroz, and J. Hofmann, Magnetic field suppression of tomographic electron transport, Phys. Rev. B 111, 155434 (2025).
- [40] T. Holder, R. Queiroz, T. Scaffidi, N. Silberstein, A. Rozen, J. A. Sulpizio, L. Ella, S. Ilani, and A. Stern, Ballistic and hydrodynamic magnetotransport in narrow channels, Phys. Rev. B 100, 245305 (2019).
- [41] J. Estrada-Álvarez, F. Domínguez-Adame, and E. Díaz, Alternative routes to electron hydrodynamics, Commun. Phys. 7, 138 (2024).
- [42] P. S. Alekseev and A. P. Dmitriev, Hydrodynamic magnetotransport in two-dimensional electron systems with macroscopic obstacles, Phys. Rev. B 108, 205413 (2023).
- [43] P. S. Alekseev and M. A. Semina, Ballistic flow of twodimensional interacting electrons, Phys. Rev. B **98**, 165412 (2018).
- [44] See Supplemental Material at http://link.aps.org/supplemental/10.1103/xsjh-lq5h for further details.
- [45] M. Müller, M. Bräuninger, and B. Trauzettel, Temperature dependence of the conductivity of ballistic graphene, Phys. Rev. Lett. 103, 196801 (2009).

- [46] Y.-T. Tu and S. Das Sarma, Wiedemann-franz law in graphene, Phys. Rev. B **107**, 085401 (2023).
- [47] A. Tomadin, G. Vignale, and M. Polini, Corbino disk viscometer for 2D quantum electron liquids, Phys. Rev. Lett. 113, 235901 (2014).
- [48] P. S. Alekseev and A. P. Alekseeva, Transverse magnetosonic waves and viscoelastic resonance in a two-dimensional highly viscous electron fluid, Phys. Rev. Lett. 123, 236801 (2019).
- [49] A. Principi, G. Vignale, M. Carrega, and M. Polini, Bulk and shear viscosities of the two-dimensional electron liquid in a doped graphene sheet, Phys. Rev. B **93**, 125410 (2016).
- [50] U. Gran, E. Nilsson, and J. Hofmann, Shear viscosity in interacting two-dimensional Fermi liquids, arXiv:2312 .09977.
- [51] P.G. Ciarlet, The Finite Element Method for Elliptic Problems (SIAM, 2002).
- [52] D. Engwirda and D. Ivers, Off-centre Steiner points for Delaunay-refinement on curved surfaces, Computer Aided Design 72, 157 (2016).
- [53] J. Callaway, Model for lattice thermal conductivity at low temperatures, Phys. Rev. 113, 1046 (1959).
- [54] M. Müller, J. Schmalian, and L. Fritz, Graphene: A nearly perfect fluid, Phys. Rev. Lett. 103, 025301 (2009).
- [55] E. I. Kiselev and J. Schmalian, Boundary conditions of viscous electron flow, Phys. Rev. B 99, 035430 (2019).
- [56] J. Maki, U. Gran, and J. Hofmann, Odd-parity effect and scale-dependent viscosity in atomic quantum gases, Commun. Phys. 8, 319 (2025).
- [57] E. Nilsson, U. Gran, and J. Hofmann, Nonequilibrium relaxation and odd-even effect in finite-temperature electron gases, Phys. Rev. X 15, 041007 (2025).
- [58] J. Hofmann and S. Das Sarma, Collective modes in interacting two-dimensional tomographic fermi liquids, Phys. Rev. B 106, 205412 (2022).
- [59] J. Hofmann and U. Gran, Anomalously long lifetimes in two-dimensional Fermi liquids, Phys. Rev. B 108, L121401 (2023).
- [60] Q. Hong, M. Davydova, P. J. Ledwith, and L. Levitov, Superscreening by a retroreflected hole backflow in tomographic electron fluids, Phys. Rev. B 109, 085126 (2024).
- [61] P. S. Alekseev and A. P. Dmitriev, Viscosity of twodimensional electrons, Phys. Rev. B 102, 241409(R) (2020).

- [62] P. J. Ledwith, H. Guo, and L. Levitov, The hierarchy of excitation lifetimes in two-dimensional Fermi gases, Ann. Phys. (Amsterdam) 411, 167913 (2019).
- [63] S. Kryhin and L. Levitov, Two-dimensional electron gases as non-Newtonian fluids, Low Temp. Phys. 49, 1402 (2023).
- [64] S. Kryhin, Q. Hong, and L. Levitov, Linear-in-temperature conductance in two-dimensional electron fluids, Phys. Rev. B 111, L081403 (2025).
- [65] G. A. Starkov and B. Trauzettel, Anomalous Knudsen effect signaling long-lived modes in 2D electron gases, arXiv: 2502.04880.
- [66] Y. Zeng, H. Guo, O. M. Ghosh, K. Watanabe, T. Taniguchi, L. S. Levitov, and C. R. Dean, Quantitative measurement of viscosity in two-dimensional electron fluids, arXiv:2407 .05026.
- [67] R. N. Gurzhi, A. N. Kalinenko, and A. I. Kopeliovich, Electron-electron momentum relaxation in a two-dimensional electron gas, Phys. Rev. B 52, 4744 (1995).
- [68] J. Hofmann and H. Rostami, Nonlinear thermoelectric probes of anomalous electron lifetimes in topological Fermi liquids, Phys. Rev. Res. 6, L042042 (2024).
- [69] I. Moiseenko, E. Mönch, K. Kapralov, D. Bandurin, S. Ganichev, and D. Svintsov, Testing the tomographic Fermi liquid hypothesis with high-order cyclotron resonance, Phys. Rev. Lett. 134, 226902 (2025).
- [70] Y. Zhu and S. Granick, Limits of the hydrodynamic no-slip boundary condition, Phys. Rev. Lett. 88, 106102 (2002).
- [71] N. Dongari, A. Sharma, and F. Durst, Pressure-driven diffusive gas flows in micro-channels: From the Knudsen to the continuum regimes, Microfluid. Nanofluid. 6, 679 (2009).
- [72] W. Huang, T. Paul, K. Watanabe, T. Taniguchi, M. L. Perrin, and M. Calame, Electronic Poiseuille flow in hexagonal boron nitride encapsulated graphene field effect transistors, Phys. Rev. Res. 5, 023075 (2023).
- [73] M. J. M. de Jong and L. W. Molenkamp, Hydrodynamic electron flow in high-mobility wires, Phys. Rev. B **51**, 13389 (1995).
- [74] L. W. Molenkamp and M. J. M. de Jong, Electron-electronscattering-induced size effects in a two-dimensional wire, Phys. Rev. B **49**, 5038 (1994).